Research Article
Open Access
CrossMark

Electrical and magnetic response of a phosphate glass - $NiFe_2O_4$ composite. A novel magnetic sensor design

Abstract

$NiFe_2O_4$ spinel – phosphate (Bi-Ba-Li) glass composite was synthesized by solid-state reaction. New crystalline magnetic phases was developed inside the glassy matrix through a controlled heat treatment. New NF-LBPB4_magnetic nanocomposite material was study. Complex impedance analysis has shown that mobile ions inside the matrix induce the development of complementary crystalline phases resulting in a composite material with excellent magnetic response. An innovative homemade device was designed to test the nanocomposite magnetic response.

Volume 3 Issue 1 - 2019

PE di Prátula,[1] Pistonesi CA,[2] Anton MA,[2] HR di Prátula,[2] Guillermo E,[2] Frechero MA[1]
[1]Departamento de Química, Universidad Nacional del Sur, INQUISUR-CONICET, Argentina
[2]Universidad Tecnolóigica Nacional, Argentina

Correspondence: Frechero MA, Grupo de Fisicoquímica de conductores iónicos de estado sólido, GFCIES, Departamento de Química, Universidad Nacional del Sur, INQUISUR-CONICET, Av. Alem 1253, CP 8000 - Bahía Blanca, Argentina, Tel +54 0291 459-5100 (3528), Email frechero@uns.edu.ar

Received: December 22, 2018 | **Published:** January 29, 2019

Introduction

Nowadays, magnetic nanoparticles materials increase their interest because they lead to new technological applications. A step forward is magnetic-glassy nanocomposite materials because they give the opportunity to obtain devices with very different shapes retaining their electrical and magnetic behaviour. Additionally, glassy matrix acts as a protection of the nanocrystalline magnetic material.[1–4] Glass-ceramics combined with multi ferroic phases have many device applications as control the magnetic state via local electric fields, the combination of ferroelectric and ferromagnetic phases allows store information on the basis of their polarization[5] encoded in the direction of the electric polarization and magnetization, yielding spintronics and non-volatile data storage, multistate permanent memory device.[6,7] Some works have reported the development of such materials: Bi_2O_3–Fe_2O_3–BaO–B_2O_3 in which $BiFeO_3$ phase was crystallizable given a glass-ceramics;[8] nanocomposites containing nanocrystals of Te_2NiMnO_6 synthesized by heat treatment[9] etc. The synthesis of nanoparticles is a complex process, and there are many different techniques for producing them.[10] Liquid phase synthesis remains one of the most common methods by the co-precipitation method. Nanoparticles can be oxide nanoparticles produced directly and by a precursor that is then subjected to an additional post-processing.[11] In this work, we have synthesized $NiFe_2O_4$ by the solid-state reaction method followed by a combination with a $42Li_2O$ 18BaO ($36P_2O_5$ $4Bi_2O_3$) glass that allows us grows new crystalline magnetic phases inside the glassy matrix through a controlled heat treatment resulting in a magnetic nanocomposite material. We have study its structural features and its magnetic its magnetic and electrical behavior.

Material synthesis

$NiFe_2O_4$ [NF] synthesis

In this work NF ($NiFe_2O_4$) pure powder was prepared by solid-state reaction method. $NiCO_3$ (II) (Riedel-de Haen AG. Seelze-Hannover) and Fe_2O_3 (Sigma-Aldrich ≥99%) powder were use to synthesize NF. Starting from the nominal composition every component was weighted and mixed in an agate mortar. The powders were well mixed and placed in a platinum crucible and decarboxylated at 800ºC for 2h in an air atmosphere and followed by 2h at 1100ºC. The obtained powder was pressed in pellets of 10 mm diameter and 2mm thickness at 10.2 metric ton/cm^2 and sintered at 700ºC for 2h. Finally, the pellets were grind again.[12–15] The crystal structure was characterized by X-ray diffraction (Philips X Pert Pro) in continuous scan mode with a copper anode (45K-30mA, Cu K_α radiation: λ=1.54Å) at room temperature in the 2θ range: 10°-90°.

Phosphate glasses synthesis

Ternary glasses of composition: 19BaO ($74P_2O_5$ $7Bi_2O_3$) and $42Li_2O$ 18BaO ($36P_2O_5$ $4Bi_2O_3$) (mol%) was prepared by a standard melt quenching technique. From now [LBPB] and [LBPB4].[16]

Composites NF-LBPB synthesis

The prepared glasses were ball-milled and the resulted powder was sieved with a 150μm mesh sieve to obtain the small fraction of particles. The glassy powder was mixed with NF powder in a ratio of: 89%wt/11%wt. The mix was heated at 700ºC for 30min.

Composite NF-LBPB4 synthesis

Powdered [LBPB4] glass was mixed with a [NF] in a ratio of 89%wt to 11%wt respectively. Both powders were mixed in an agate mortar a new glassy material was prepared by the standard melt quenching technique. First, it was heated for 1 h a 1353K, shaken frequently to ensure homogenization. The melt was poured on an aluminum plate at 0ºC and the obtained solid drops were held for two hours a 473K to remove the mechanical stress and 3hrs at 703K to allow the grows of [NF] crystallites inside the glassy matrix.[17,18]

Materials characterization and results

Structural

The glassy nature of the resulting solids by quenching technique was tested using X-ray diffraction (XRD) analysis and differential temperature analysis (DTA). DTA curves were recorded using a Rigaku Thermoflex TG 8110 associated with Thermal Analysis Station TAS 100, the T_g (glass transition temperature) of each sample was determined with a heating rate of 10K min^{-1} in the range 25ºC to 400ºC using 20–30 mg of glass samples finely grounded in an agate mortar.[19] Figure 1 shows the X-ray diffraction patterns that confirms the single phase material. All the diffraction peaks can be indexed to the cubic spinel structure of JCPDS card no. 74-2081 with the presence of (220), (311), (400), (422), (511), (440), and (622) planes, with small proportion of impurities. The lattice parameter was in good agreement with standard value. Figure 2 & Figure 3 show the DTA scan and the corresponding T_g for each glassy sample. From the results in these figures we learn that the T_g value decreases 10% when lithium oxide is incorporated in the phosphate glassy matrix. Also, Figure 3 shows two extra peaks after its T_g which belong to the devitrification phenomenon.

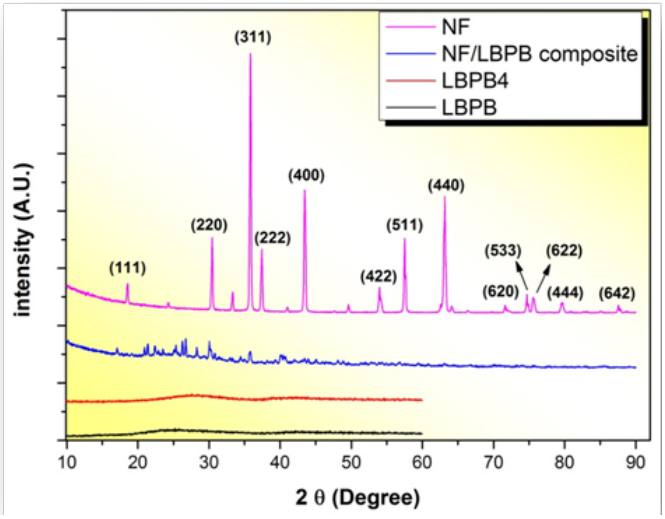

Figure 1 [NF] X-ray diffraction pattern (pink); NF/LBPB composite (blue) X-ray diffraction pattern; [LBPB4] (red) and [LBPB] (black) X-ray diffraction pattern.

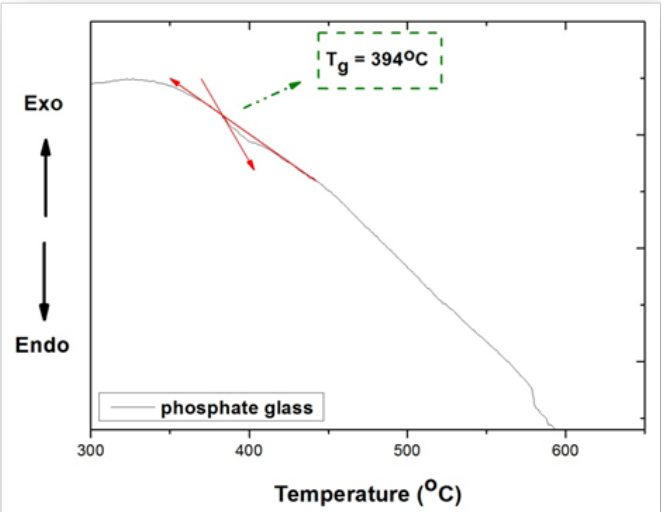

Figure 2 [LBPB] DTA heating curve.

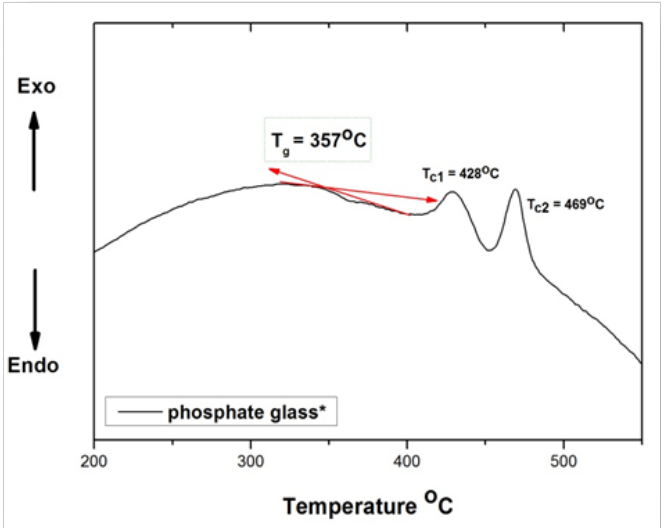

Figure 3 [LBPB4] DTA heating curve.

Electrical properties

Every glassy sample was polished with a sand paper to obtain disks with two parallel mirror surfaces with thickness ranging between 0.5 to 0.7mm and coated with a thin layer of silver paint to having a proper electrical contact. Impedance measurements were carried (Agilent LCR meter 4284A; 20Hz–1MHz; AC voltage amplitude signal of 0.80V) in a temperature range between room temperature and (Tg−15)°C. Electrical measurements was done registering the magnitude of the sample impedance |Z| and the phase angle φ, using the impedance meter. Show the complex permittivity $\varepsilon'_{(\omega)}$ and the dielectric loss (tan δ) measured as a function of the temperature for the pristine composite NF-LBPB4 and NF/LBPB4 treated 1h to 703K. The values of the complex permittivity are calculated using the following equations:

$$\varepsilon' = \frac{\frac{L}{A} * \frac{\operatorname{sen}\theta}{|Z|} * 100}{f * 2 * \pi * \varepsilon_o} \quad (1)$$

$$\varepsilon'' = \frac{\frac{L}{A} * \frac{\cos\theta}{|Z|} * 100}{f * 2 * \pi * \varepsilon_o} \quad (2)$$

In these expressions ε' is the real part of the complex permittivity characterizes the energy stored in the material and, ε'' is the imaginary part and represents the energy losses by the material; ε_0 is the free space permittivity ($8.854*10^{-12}$ F. m^{-1}); (L/A) the geometric factor; *f*, the frequency.

The dielectric loss is obtained from the relation: $\tan\delta = \frac{\varepsilon''}{\varepsilon'}$ (3)

Figure 4 shows that the ε' is lower when the material is heat treated and also the dielectric loss which decrease more confirming lower energy losses than in the pristine sample. The Maxwell - Wagner model for the heterogeneous structure explain σ the ε' dispersion phenomenon observed at low frequency. We assume that the grain boundary present in the composite are smoothed after the heat treatment due to a cation interchange between the combined materials. Additionally, Figure 5A & Figure 5B show that after the heat treatment crystallites are larger enough to be revealed by a second resistance response clearly observed in Figure 5B. However, as we mentioned above the interface between both materials is less

bloquing as the conductivity spectra showed in Figure 6A & Figure 6B while the σ_{dc} is low after the heating confirming that mobile ions in the glassy matrix are trapped around the crystalline phase given new crystalline structures as X-ray diffraction pattern shows in Figure 1.

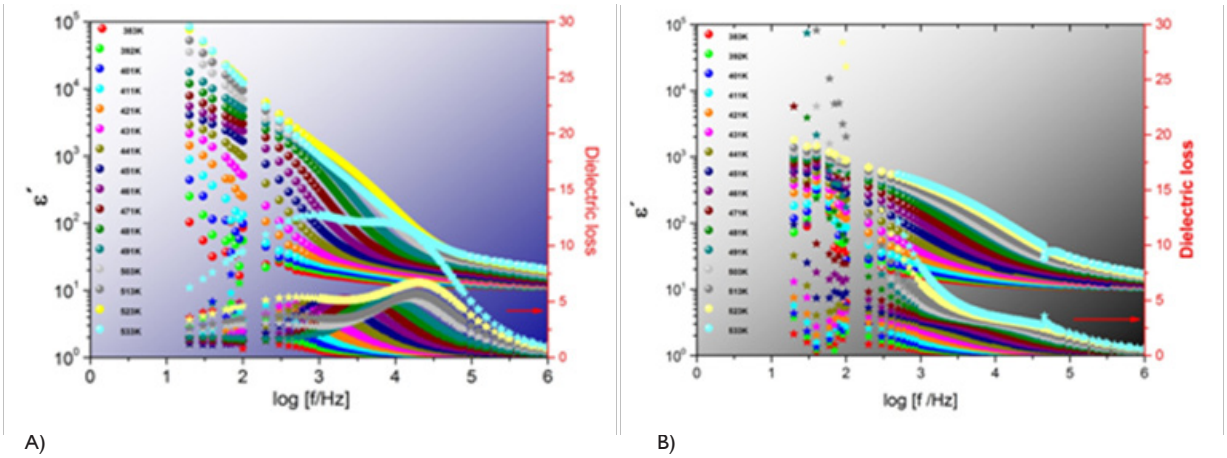

A) B)

Figure 4 Real part of the complex permittivity of: A)NF-LBPB4 pristine composite and B) NF-LBPB4 treated 1 h at 703K.

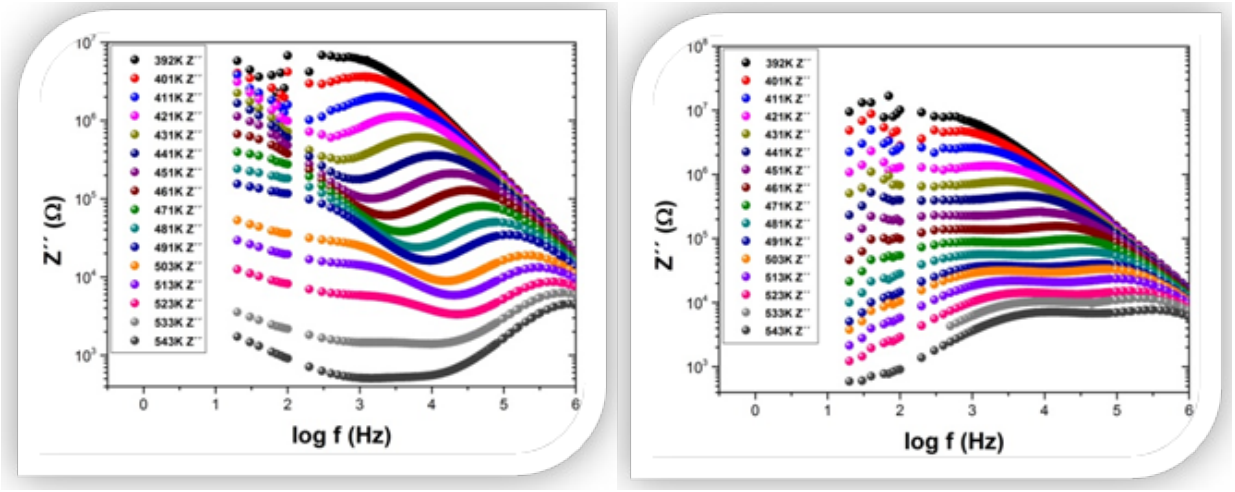

A) B)

Figure 5 Impedance imaginary part: A) NF-LBPB4 pristine composite and B) NF-composite heat treated.

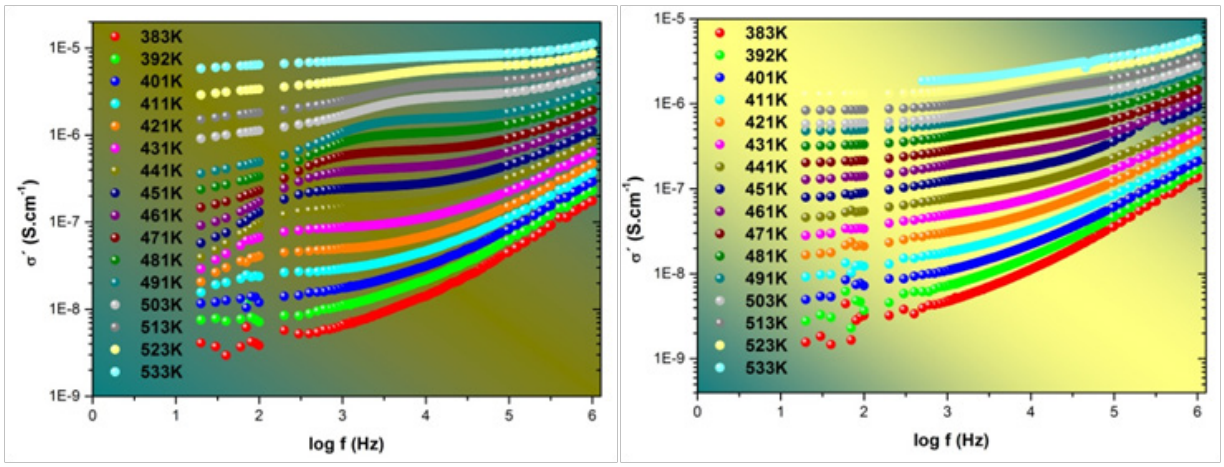

A) B)

Figure 6 Conductivity spectra: A) NF-LBPB4 pristine composite and B) NF-LBPB4 heat treated.

Citation: Prátula PE, Pistonesi CA, Anton MA, et al. Electrical and magnetic response of a phosphate glass - $NiFe_2O_4$ composite. A novel magnetic sensor design. *Material Sci & Eng.* 2019;3(1):13–19. DOI: 10.15406/mseij.2019.03.00082

Magnetic properties

Figure 7 shows the magnetization loops (T-H) measured at room temperature.[20] It exhibits typical ferromagnetic behavior and it reaches a saturation magnetization values 3Ms (pristine composite; glass ceramic)≈ Ms (heat treated composite, after 1 or 2hours). The composite prepared as a glass-ceramic has the same response as the pristine composite. In order to obtain such response we have design a homemade magnetic analyzer. A sensor with a fine adjustment screw type system was built like describe the following Figure 8(A-D), using the same circuit, the measurement is made with air core and winding of 100/100turns.[21,22] The magnetization curve of each material is determined based on which the flow is determined by the supply voltage. The circuit used is shown in Figure 8:

$$\left|V_i\right| = 4,44 * f * N_s * \Phi máx \;.\; \Rightarrow .\Phi máx = \frac{\left|V_i\right|}{4,44 * f * N_s} \quad (4)$$

$$H = \frac{N_P . I_i}{l_j} \quad (5)$$

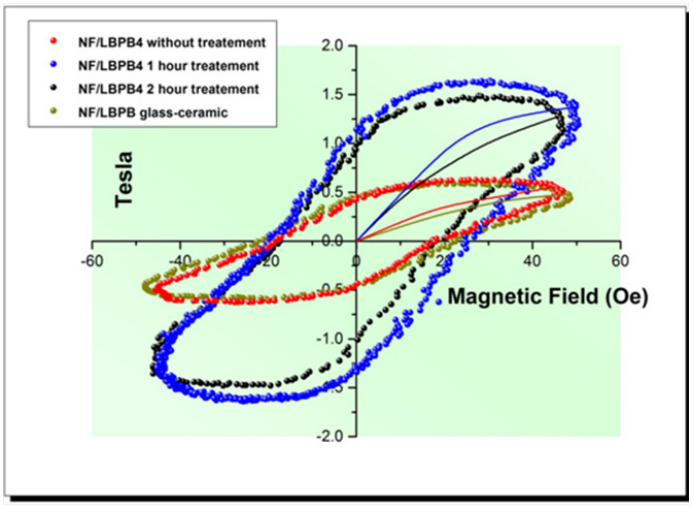

Figure 7 Magnetic hysteresis loops at room temperature of NF-LBPB4 composites pristine and heat treated at different times.

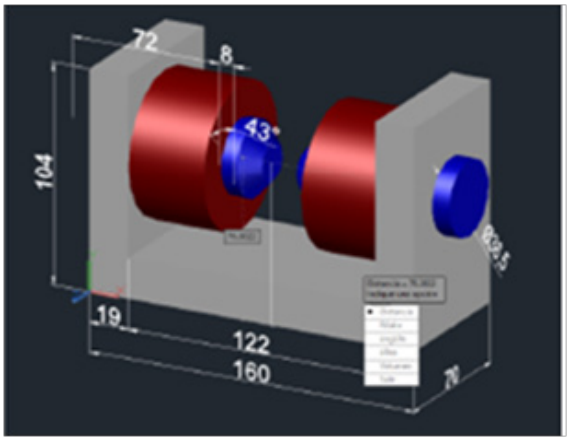

A)

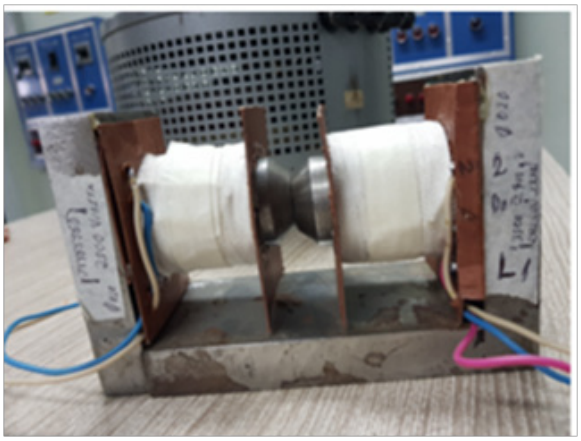

B)

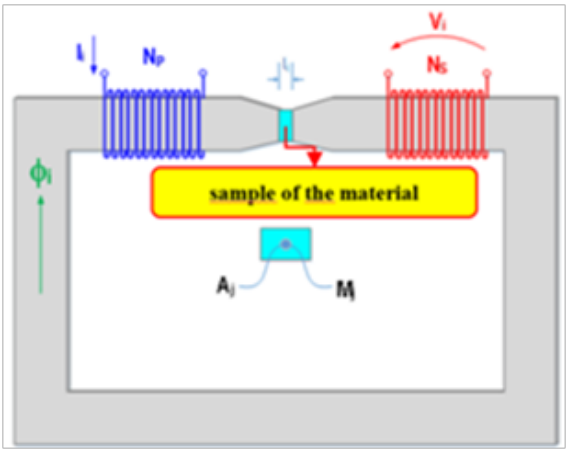

C)

D)

Figure 8 A) Sensor design; B) Sensor built; C) sample location; D) oscilloscope ScopeMeter Fluke199) 200 MHz 2.5 GS / s, double input.

The current is measured on the primary winding and the voltage on the secondary winding, thus achieving that both values are not affected by the insertion of the instruments. The current determines the magneto motive force and the voltage the conversion flow. A device was designed to check the operational material behavior using 0.27mm thick oriented grain iron as reference. The system has the

Citation: Prátula PE, Pistonesi CA, Anton MA, et al. Electrical and magnetic response of a phosphate glass - $NiFe_2O_4$ composite. A novel magnetic sensor design. *Material Sci & Eng.* 2019;3(1):13–19. DOI: 10.15406/mseij.2019.03.00082

following components:

A. Drag system of neodymium magnets.

B. Device where the samples are placed and voltage taken.

C. The programmable control automaton (Figure 9).

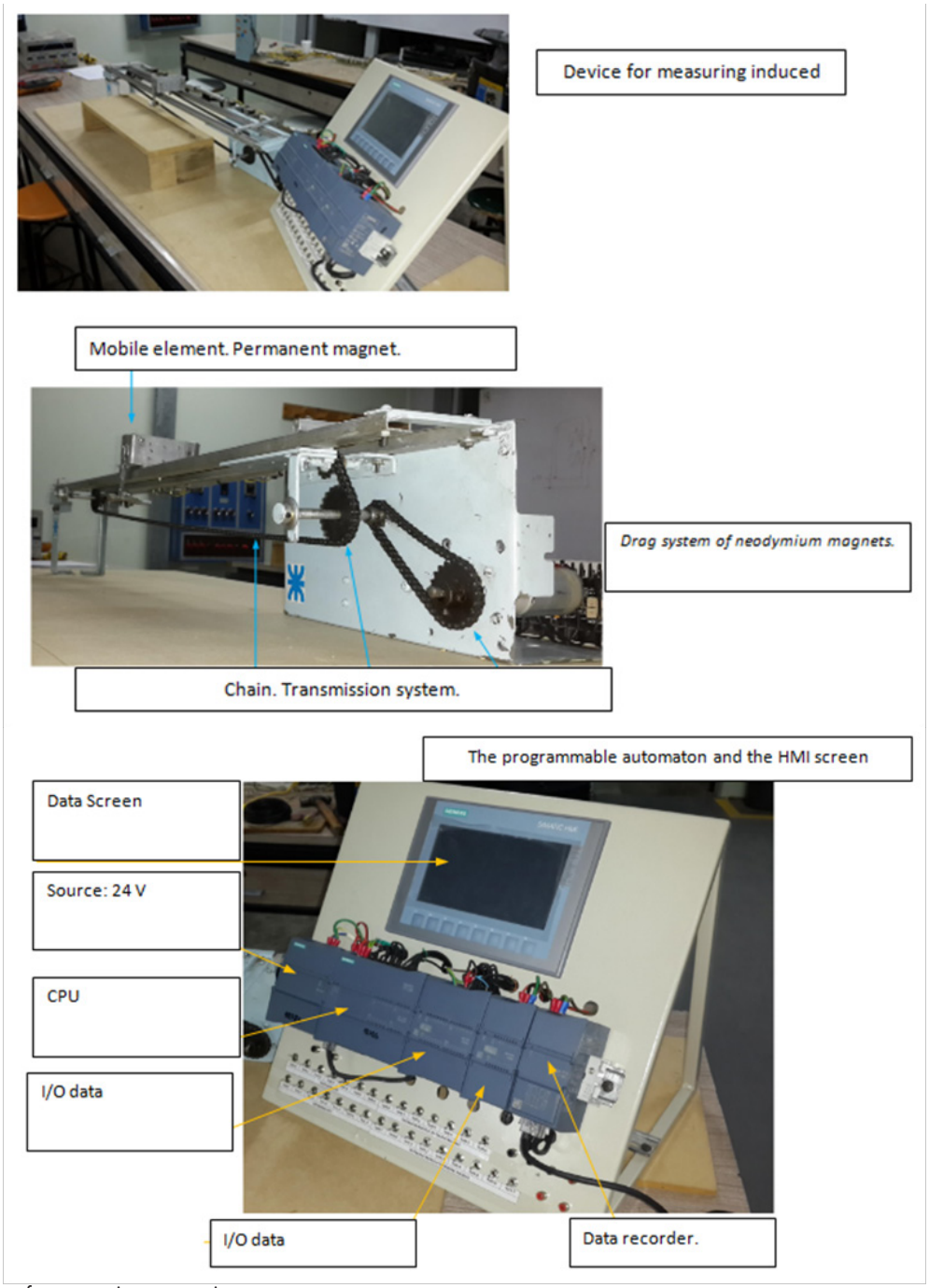

Figure 9 Novel devices for comparison magnetic response.

The device has a 24 volt direct current motor, rack and chain system that convert the rotary movement into linear. The system has a permanent magnet and limits of career and position sensors for the movement and measurement.[23,24] Also, the system has a second element where the samples are placed and where is the voltage induced. The voltage generated by the samples is compared to the passage of the permanent magnets. We use first silicon steel whose characteristics are well known and next our glassy composite materials. It is important to emphasize that both shape and dimensions of samples are thoroughly determined. The generated voltage on the driver depends on the magnetic field intensity due to the speed of the magnets and the magnetic circuit that surrounds the driver. As an example, Figure 10 shows the result of one measure.

First signal of 7.20 10^{-3} s – Intensity: from 2mV to 50mV

Second signal of 8.40 10^{-3} s – Intensity: from 2mV a 194mV

We took 9727 measurements during 3843 seconds in order to obtain an average response.

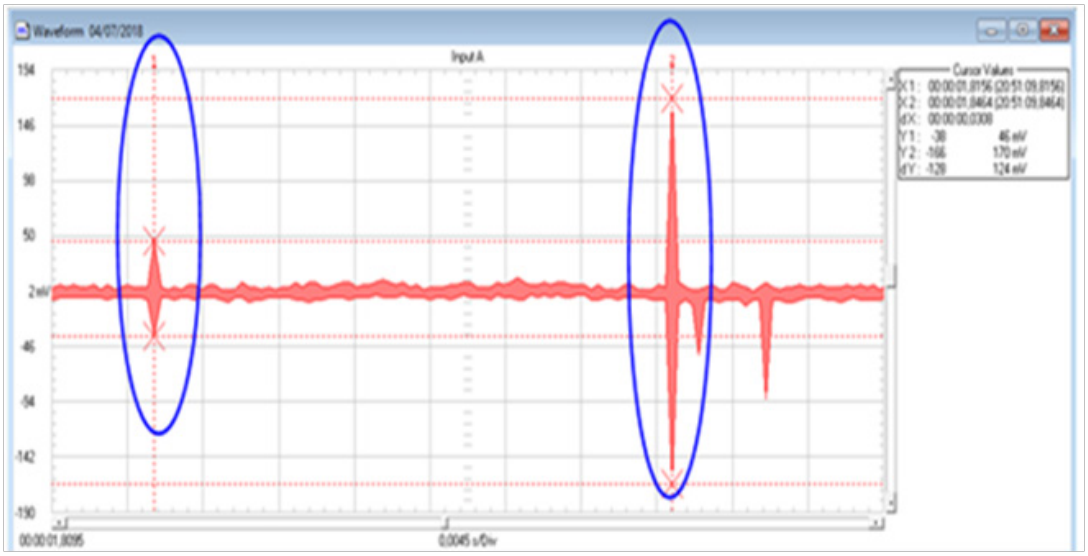

Figure 10 Comparative voltage measured of two series conductors: silicon steel—glassy composite material (NF-LBPB4).

Discussion

The growth of the crystalline phase inside the glassy matrix improves the magnetic response of the composite material. The resulting material's T_g is high enough to permit the proposed technological use. From the electrical results we show that a smooth inter phase between the magnetic crystallites and the glassy matrix is obtain after an appropriated heat treatment assisted by the cation interchange. The crystallites obtained are larger enough to be observed and the mobile ions in the glassy matrix trapped around the crystalline phase give a new crystalline structures. As a result, the composite material developed has the advantages of the glassy materials with the magnetic properties necessary to be applied in green electrical generation for example (as part of a stator). The innovative homemade device designed allows the magnetic characterization of our composite material. Considering that it was built with standard laboratory equipment, it is an excellent opportunity to test the material performance in comparison to very well known magnetic materials as for example silicon steel that we used.

Conclusion

In this work we synthesized the $NiFe_2O_4$ spinel by solid-state reaction and the phosphate (Bi-Ba-Li) glass by melt quenching technique. Applying a mechanical mix and several heat treatments an innovative nanocomposite was developed. Additionally, the heat treatments led to growth new crystalline magnetic phases inside the glassy matrix. The NF-LBPB4 magnetic nanocomposite material was thoroughly study. Complex impedance analysis allows to evidence that are the cations inside the matrix which induce the development of complementary crystalline phases. The composite material obtained has an excellent magnetic response. In order to evaluate the composite magnetic behavior an innovative homemade device was designed. We present technical details to build it.

Acknowledgments

Financial support by CONICET (PIP 11220120100010CO), ANPCyT (PICT 2016-0101), UNS. M.MdeL.S. CPI English assistance. P.E.dP. is CONICET fellowship and M.A.F is CONICET Research Fellows, Argentina.

Conflicts of interest

Author declares that there is no conflict of interest.

References

1. Takahashi Y, Meguro K, Naganuma H, et al. Multiferroic $BiFeO_3$ glass-ceramics: Phase formation and physical property. *Appl Phys Lett*. 2014;104:221901.
2. Chen DQ, Xiang WD, Liang XJ, et al. Advances in transparent glass–ceramic phosphors for white light-emitting diodes—A review. *J Eur Ceram Soc*. 2015;35:859–869.
3. Wang XG, Zhang Y, Zhu J, et al. *Ceram Int*. 2014;40:16557–16562.
4. Zeng HD, Liu Z, Jiang Q, et al. Large third-order optical nonlinearity of $ZnO–Bi_2O_3–B_2O_3$ glass–ceramic containing $Bi_2ZnB_2O_7$ nanocrystals. *J Eur Ceram Soc*. 2014;34:4383–4388.
5. Scott JF. Data storage: multiferroic memories. *Nat Mater*. 2007;6(4):256–257.
6. Gajek M, Bibes M, Fusil S, et al. Tunnel junctions with multiferroic barriers. *Nat Mater*. 2007;6:296–302.
7. Yang F, Tang MH, Ye Z, et al. Eight logic states of tunneling magnetoelectroresistance in multiferroic tunnel junctions. *J Appl Phys*. 2007;102:044504.
8. Takahashi Y, Meguro K, Naganuma H, et al. Multiferroic $BiFeO_3$ glass-ceramics: Phase formation and physical property. *Appl Phys Lett*. 2014;104:221901.
9. Maiti RP, Basu S, Bhattacharya S, et al. Multiferroic behavior in glass–crystal nanocomposites containing Te_2NiMnO_6. *J Alloy Compd*. 2011;509:6056–6060.
10. Chaudhuri RG, Paria S. Core/Shell Nanoparticles: Classes, Properties, Synthesis Mechanisms, Characterization, and Applications. *Chem Rev*. 2012;112:2373–2433.
11. Cushing BL, Kolenichenko VL, O'Connor CJ. Recent Advances in the Liquid-Phase Syntheses of Inorganic Nanoparticles. *Chem Rev*. 2004;104:3893–3946.
12. Yan Chen, Qiong Wu, Qiutong Jin, et al. A facile sol-gel method for the fabrication of nitrogen doped $TiO_2/NiFe_2O_4$/diatomite composite with enhanced photoactivity. *Advanced Powder Technology*. 2017;28:2225–2231.

13. Patil JY, Nadargi DY, Gurav JL, et al. Synthesis of glycine combusted $NiFe_2O_4$ spinel ferrite: A highly versatile gas sensor. *Materials Letters*. 2014;124:144–147.

14. Ali Bahadur, Aamer Saeed, Muhammad Shoaib, et al. Eco-friendly synthesis of magnetite (Fe_3O_4) nanoparticles with tunable size: Dielectric, magnetic, thermal and optical studies. *Materials Chemistry and Physics*. 2017;198:229–235.

15. Anita Sudhaika, Pankaj Raizadaa, Pooja Shandilya, et al. Magnetically recoverable graphitic carbon nitride and $NiFe_2O_4$ based magnetic photocatalyst for degradation of oxytetracycline antibiotic in simulated wastewater under solar light. *Journal of Environmental Chemical Engineering*. 2018;6:3874–3883.

16. Di prátuñ**a** PE, Terny S, Sola ME, et al. *Research and Reviews in Materials Science and Chemistry*. 2016;7(1):25–42.

17. Pratthana Intawina, Wilaiwan Leenakulc, Pongsakorn Jantaratanad, et al. Synthesis, structural and electrical properties of granular BT-NZF nanocrystals in silicate glass. *Ceramics International*. 2017;43:S258–S264.

18. Othmana HA, Eltabeyb MM, Samia E Ibrahima, et al. *Elkholya Physica B*. 2017;506:115–121.

19. Qiang Zhao, Huaiwu Zhang, Fang Xu, et al. Low-temperature sintering and magnetic properties of MABS glass doped Li0.35Zn0.30Mn0.05Ti0.1Fe2.05O4 ferrites. *Journal of Alloys and Compounds*. 2018;764:834–839.

20. Vishal K Chakradhary, Azizurrahaman Ansaria, Jaleel Akhtar M. Design, synthesis, and testing of high coercivity cobalt doped nickel ferrite nanoparticles for magnetic applications. *Journal of Magnetism and Magnetic Materials*. 2019;469:674–680.

21. Di Prátula HR, Marisa A Frechero, Andres Garcia, et al. 2nd Sustainable Energy Congress in Bahía Blanca. 2016:448–456.

22. Dmitry Svechkarenko. On Analytical Modeling and Design of a Novel Transverse Flux Generator for Offshore Wind Turbines. Licentiate Thesis Stockholm, Sweden; Royal Institute of Technology: 2007.

23. Dmitry Svechkarenko, Juliette Soulard, Chandur Sadarangani. Parametric study of a transverse flux wind generator at no-load using three-dimensional finite element analysis. Tokyo, Japan; IEEE: 2009.

24. Gene Shane Liew, Nesimi Ertugrul, Wen Liang Soong, et al. Investigation of axial field permanent magnet motor utilising amorphous magnetic material. *Australian Journal of Electrical and Electronics Engineering*. 2007.